

Article

TiO₂/ZnO Nanofibers Prepared by Electrospinning and Their Photocatalytic Degradation of Methylene Blue Compared with TiO₂ Nanofibers

Chang-Gyu Lee ¹, Kyeong-Han Na ¹, Wan-Tae Kim ¹ , Dong-Cheol Park ^{1,2}, Wan-Hee Yang ² and Won-Youl Choi ^{1,3,*}

¹ Department of Advanced Materials Engineering, Gangneung-Wonju National University, Gangneung, Gangwon 25457, Korea

² WITH M-TECH Co., Ltd., Suwon, Gyeonggi 16229, Korea

³ Research Institute for Dental Engineering, Gangneung-Wonju National University, Gangneung, Gangwon 25457, Korea

* Correspondence: cwy@gwnu.ac.kr

Received: 19 July 2019; Accepted: 16 August 2019; Published: 19 August 2019



Abstract: TiO₂ nanofibers have high chemical stability and high strength and are applied to many fields such as air pollution sensors and air pollutant removal filters. ZnO nanofibers also have very high absorptivity in that air and are used as germicides and ceramic brighteners. TiO₂/ZnO nanofibers, which have a composite form of TiO₂ and ZnO, were fabricated and show higher photocatalytic properties than existing TiO₂. The precursor, including zinc nitrate hexahydrate, polyvinyl acetate, and titanium isopropoxide, was used as a spinning solution for TiO₂/ZnO nanofibers. Electrospun TiO₂/ZnO nanofibers were calcined at 600 °C and analyzed by field emission scanning electron microscope (FE-SEM) and X-ray diffraction (XRD). The average diameter of TiO₂/ZnO nanofibers was controlled in the range of 189 nm to 1025 nm. XRD pattern in TiO₂/ZnO nanofibers have a TiO₂ anatase, ZnO, Ti₂O₃, and ZnTiO₃ structure. TiO₂/ZnO nanofibers with a diameter of 400 nm have the best photocatalytic performance in the methylene blue degradation experiments and an absorbance decrease of 96.4% was observed after ultraviolet (UV) irradiation of 12 h.

Keywords: TiO₂ nanofibers; TiO₂/ZnO nanofibers; electrospinning; photocatalyst

1. Introduction

There is a growing concern about air pollution due to internal combustion engines installed in vehicles and the large amount of exhaust gas generated in various industrial fields. Typical air pollutants include volatile organic compounds which are known to be very harmful to the human body. The World Health Organization (WHO) has announced that the incidence of various respiratory diseases can be lowered by reducing air pollution. Air pollution will become more and more serious as the scale of various industries increases. Accordingly, various solutions for reducing the concentrations of pollutants in the air such as microorganisms, photocatalysts, and activated carbon have been proposed. Among them, photocatalyst technology has attracted attention because it can continuously decompose pollutants by using renewable energy [1–3]. A photocatalytic method has been studied as a method of removing pollutants. A photocatalyst means that the oxidation-reduction reaction on the surface of a substance occurs by absorbing light. It is applied to various tasks such as decomposition of harmful substances by the oxidation-reduction reaction that occurs on the surface, gas detection, ultraviolet blocking, antibacterial function, and midnight function. The photocatalytic reaction does not require other energy because the reaction is also caused by solar energy and light. Since CO₂ and H₂O generated by these photocatalytic reactions do not pollute the environment,

they are environmentally friendly and economical because they can be used semipermanently [4–7]. Many TiO₂ nanomaterials and ZnO nanomaterials are used as these photocatalyst materials [8–15]. This is because TiO₂ nanomaterials are very stable physically and chemically and have excellent heat resistance and bio-friendly properties [16–19]. ZnO nanomaterials have a high degree of adsorption and are used as ceramic brighteners, germicides, and the like [20–23].

Nanomaterials such as nanofibers, nanotubes, and nanoparticles have various physical and chemical properties because they have various structures and pore distribution [24–26]. Among such nanomaterials, one-dimensional nanomaterials have different properties from bulk materials and have been studied in various fields for the application of chemical sensors, photovoltaic cells, optical filters, and improvement of catalytic activity [27–33]. Nanofibers have excellent photocatalytic and electrical properties because of their large specific surface area and one-dimensional structure [34–37]. The electrospinning process is a practical technique with a low cost and high efficiency, and many studies have reported producing these various nanofibers [38–43]. In the electrospinning process, the precursor solution flows through at a constant rate through a pump in such a way as to create a continuous nanofiber; then electrodes are connected to the inflowing electrospinning solution and other electrodes are connected to the appliance plate. At this time, if a high voltage is applied, it is emitted in a conical shape by surface tension at the electrospinning solution end. The charge is subsequently stored in the electrospinning solution, and the mutual repulsion causes the cone to be radiatively stretched to jet when the surface tension of the electrospinning solution is exceeded. In the radiation-stretched electrospinning solution, volatilization of the solvent occurs before it collects in the plate, and it is possible to obtain disorderly arranged nanofibers in the plate [44,45].

In this study, the electrospinning process was used to fabricate TiO₂/ZnO nanofibers for photocatalyst materials and process variables were controlled to obtain a stable and optimized one-dimensional structure. The microstructure and phase of the electrospun TiO₂/ZnO nanofibers were analyzed through field emission scanning electron microscopy (FE-SEM) and X-ray diffraction (XRD), respectively. The photocatalytic efficiencies of TiO₂/ZnO nanofibers and TiO₂ nanofibers were observed by ultraviolet–visible spectroscopy (UV–Vis) using the photocatalytic decomposition of methylene blue.

2. Materials and Methods

2.1. Electrospinning Process

The solution, *N,N*-Dimethylformamide (DMF, extra pure, DAEJUNG Chemicals and Metals Co., Ltd., Siheung-Si, Korea), was used as a solvent for dissolving a polyvinyl acetate (PVAc, Mw~500,000 by GPC, Powder, Sigma-Aldrich Co., Ltd., St. Louis, MO, USA) and 5 wt % PVAc was dissolved. DMF solution of 5g with PVAc was stirred for 4 h using a stirrer. After dissolution was complete, 6 g titanium (IV) isopropoxide (TTIP, JUNSEI Co., Ltd., Tokyo, Japan) and 21–35 wt % acetic acid (extra pure, DAEJUNG Chemicals and Metals Co. Ltd., Siheung-Si, Korea) were added. The solution became clear and 0.1 g zinc powder (Powder, Sigma-Aldrich Co., Ltd., St. Louis, MO, USA) was added and stirred for 2 h.

Figure 1 is a diagram schematically showing the electrospinning process. The distance between the needle and the plate was 15 cm and a 10-mL syringe was used. To obtain the various microstructures of TiO₂/ZnO nanofibers, experimental variables such as voltage, inflow rate, and amount of acetic acid were controlled. The applied voltages of 12 kV, 15 kV, and 18 kV, the pump inflow rates of 1 mL/h, 0.8 mL/h, and 0.6 mL/h, and 21 wt %, 28 wt %, and 35 wt % of acetic acid were used, respectively. The electrospinning process variables for TiO₂/ZnO nanofibers are summarized in Table 1.

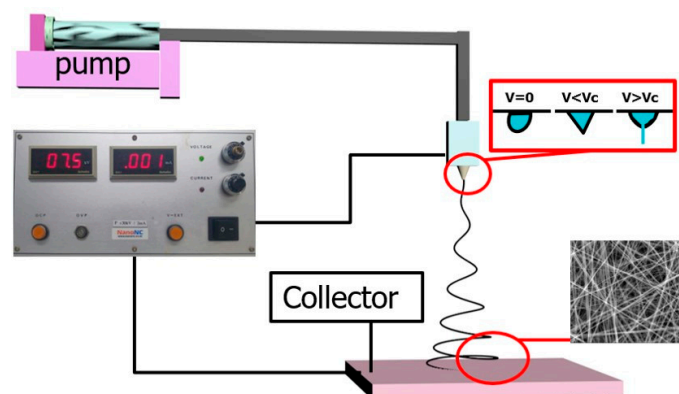


Figure 1. Schematic diagram of electrospinning process.

Table 1. Process variables of electrospinning for TiO₂/ZnO nanofibers.

Variable	Voltage (kV)	Flow Rate (mL/h)	Acetic Acid (wt %)
Voltage	12	1	21
	15	1	21
	18	1	21
Flow rate	12	1	21
	12	0.8	21
	12	0.6	21
Acetic acid	12	1	21
	12	1	28
	12	1	35

Electrospun TiO₂/ZnO nanofibers were dried at 80 °C for 24 h in an oven. The dried TiO₂/ZnO nanofibers was heat-treated at 600 °C for 1 h in a furnace. The microstructure of TiO₂/ZnO nanofibers was observed using FE-SEM (SU-70, Hitachi Co., Tokyo, Japan) and the diameters of TiO₂/ZnO nanofibers were measured. To confirm the metal oxide phase of TiO₂/ZnO nanofibers, XRD (AXS-D8, Bruker Co., Madison, WI, USA) patterns were also observed from 20° to 80° at a rate of 0.03° per step using a Cu K α target.

2.2. Evaluation of Photocatalytic Efficiency

The photocatalytic decomposition reaction was carried out using an ultraviolet lamp (JINLED Co., Ltd.) of 10 W at room temperature as an irradiation light source. The irradiation distance between the lamp and the sample was fixed to 10 cm. A nanofiber of 0.5 g was added to the methylene blue aqueous solution, and the mixture was stirred to irradiate the light source. To compare TiO₂/ZnO nanofibers with TiO₂ nanofibers, TiO₂ nanofibers were fabricated by the electrospinning process. The electrospinning process conditions for the nanofibers are shown in Table 2.

Table 2. Electrospinning process conditions of nanofibers used in the decomposition of methylene blue for photocatalytic performance evaluation.

	Voltage (kV)	Flow Rate (mL/h)	Acetic Acid (wt %)
TiO ₂ nanofibers	15	1	0
TiO ₂ /ZnO-1 nanofibers	15	3	28
TiO ₂ /ZnO-2 nanofibers	15	2	28

To fabricate TiO₂ nanofibers, polyvinylpyrrolidone (PVP, MW 1,300,000 Powder, ALFA AESAR Co., Ltd., Tewksbury, MA, USA) and ethyl alcohol (EtOH, 99.5%, SAMCHUN Chemical Co., Ltd.,

Seoul, Korea) were used. TTIP and acetylacetone (ACAC, JUNSEI Chemical Co., Ltd., Tokyo, Japan) were also added into the PVP-based solution and the mixed solution was stirred for 2 h. The prepared TiO₂ electrospinning solution was mounted on the pump and the electrospinning was conducted at the pump inlet rate of 1 mL/h and voltage of 15 kV. As-spun TiO₂ nanofibers were heat-treated at 450 °C for 3 h and TiO₂ nanofibers with an anatase phase were prepared to compare with TiO₂/ZnO nanofibers. The molar ratio of TiO₂ to ZnO was equal to 17:1 in TiO₂/ZnO-1 and TiO₂/ZnO-2 nanofibers. To obtain a different diameter, the flow rate was controlled. TiO₂/ZnO-1 and TiO₂/ZnO-2 nanofibers were fabricated at a flow rate of 3 mL/h and 2 mL/h, respectively. The prepared TiO₂/ZnO nanofibers were dried at 80 °C for 24 h. The dried specimen was placed in a heating furnace and heat-treated at 600 °C for 1 h. To evaluate the photocatalytic activity, UV-Vis spectrums with the TiO₂ and TiO₂/ZnO nanofibers were observed using the photocatalytic decomposition of methylene blue.

3. Results

3.1. TiO₂/ZnO Nanofibers

Figure 2 shows the FE-SEM images of TiO₂/ZnO nanofibers fabricated by the electrospinning process at various applied voltages of 12 kV, 15 kV, and 18 kV. TiO₂/ZnO nanofibers have a typical one-dimensional and clean microstructure without droplets. Increasing the voltage during the electrospinning process increased the charge density of the solution and nanofibers with a small diameter were obtained. When voltage exceeding the limit was applied, nanofibers were not formed and sprayed. If a lower voltage is used then surface tension is applied, and nanofibers in the form of nanofiber intermediate beads can be obtained instead of nanofibers of a constant diameter.

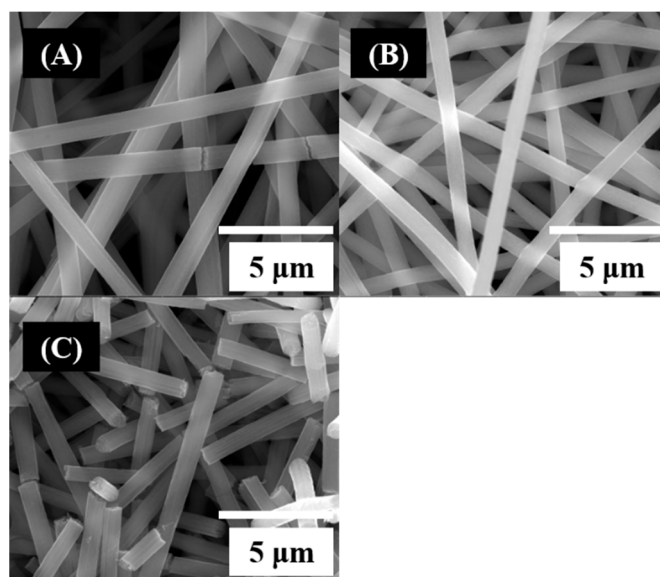


Figure 2. Field emission scanning electron microscope (FE-SEM) images of electrospinning TiO₂/ZnO nanofibers: (A) 12 kV, (B) 15 kV, and (C) 18 kV.

The average diameters of TiO₂/ZnO nanofibers with applied voltage was 1025 nm, 735 nm, and 694 nm, respectively. It reveals that the higher the voltage, the smaller the diameter. The diameters of TiO₂/ZnO nanofibers with applied voltage are plotted in Figure 3.

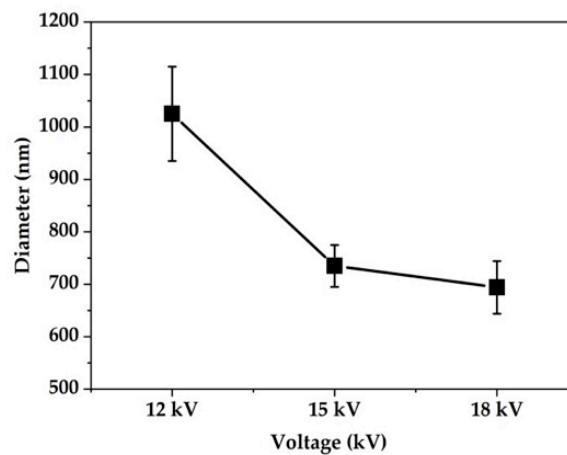


Figure 3. Average diameters of TiO₂/ZnO nanofibers with voltage.

Figure 4 shows FE-SEM images of TiO₂/ZnO nanofibers fabricated by the electrospinning process at various inflow rates of 1.0 mL/h, 0.8 mL/h, and 0.6 mL/h. A one-dimensional nanofiber was observed in all TiO₂/ZnO nanofibers. When the flow rate of the electrospinning solution is fast, the size of the droplet that forms on the tip of the needle becomes large. Even when the solution is reached at the collector, the solvent in the solution may not be completely evaporated, and a nanofiber with a bead-shape or large diameter can be obtained.

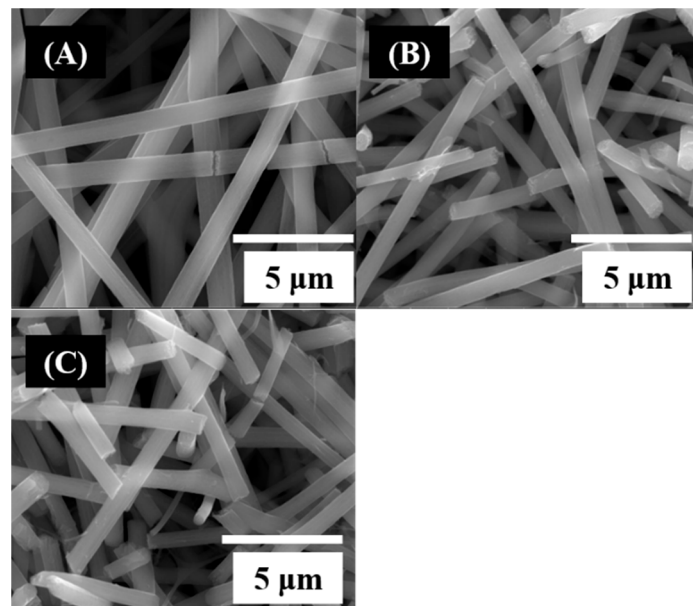


Figure 4. FE-SEM images of electrospinning TiO₂/ZnO nanofibers: (A) 1 mL/h, (B) 0.8 mL/h, and (C) 0.6 mL/h.

The average diameters of TiO₂/ZnO nanofibers with an inflow rate were 1025 nm, 771 nm, and 728 nm, respectively. The average diameter of TiO₂/ZnO nanofibers increased with inflow rate. The diameters of TiO₂/ZnO nanofibers with an inflow rate are plotted in Figure 5.

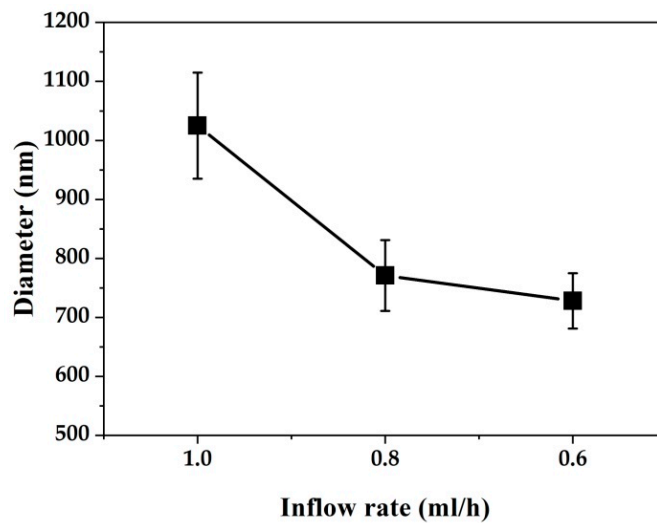


Figure 5. Average diameters of TiO_2/ZnO nanofibers with inflow rate.

Figure 6 shows FE-SEM images of TiO_2/ZnO nanofibers fabricated by the electrospinning process at various amounts of acetic acid—21 wt %, 28 wt %, and 35 wt %—in the precursor solution. All TiO_2/ZnO nanofibers have nanofiber structural networks. As the amount of acetic acid in the electrospinning solution increases, the viscosity decreases, and the diameter of the nanofibers dramatically decreases. This reveals that the viscosity is the most important parameter for controlling the diameter in the electrospinning process.

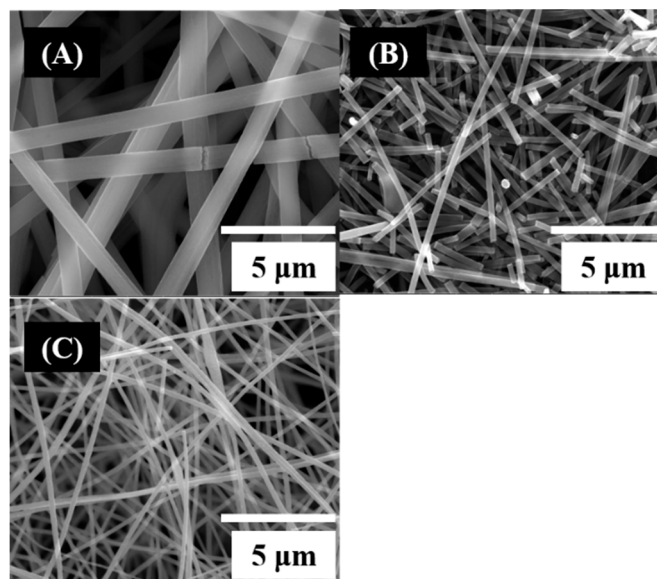


Figure 6. FE-SEM images of electrospinning TiO_2/ZnO nanofibers: (A) 21 wt %, (B) 28 wt %, and (C) 35 wt %.

The average diameters of TiO_2/ZnO nanofibers with an inflow rate were 1025 nm, 233 nm, and 189 nm, respectively and the average diameter dramatically decreased with the amount of acetic acid. The diameters of TiO_2/ZnO nanofibers with different amounts of acetic acid are plotted in Figure 7.

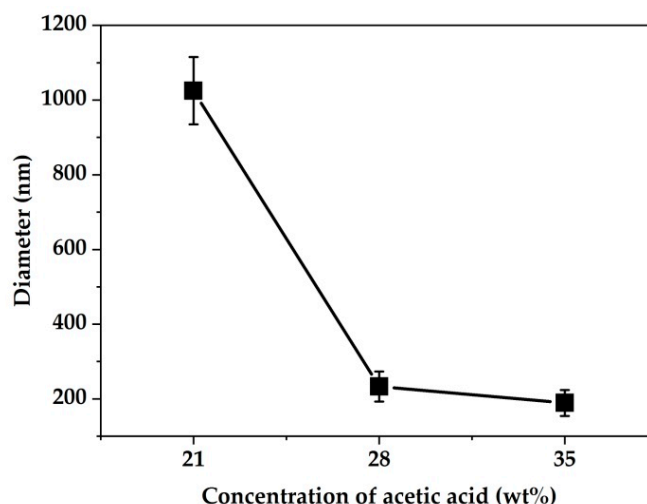


Figure 7. Average diameters of TiO₂/ZnO nanofibers according to the amount of acetic acid.

To observe the crystal phase of TiO₂/ZnO nanofibers, XRD analysis was conducted. Figure 8 shows the XRD pattern of TiO₂/ZnO nanofibers. The peaks of TiO₂ anatase, ZnO, Ti₂O₃, and ZnTiO₃ were identified and the peak of ZnTiO₃ was obtained by the reaction of TiO₂ and ZnO.

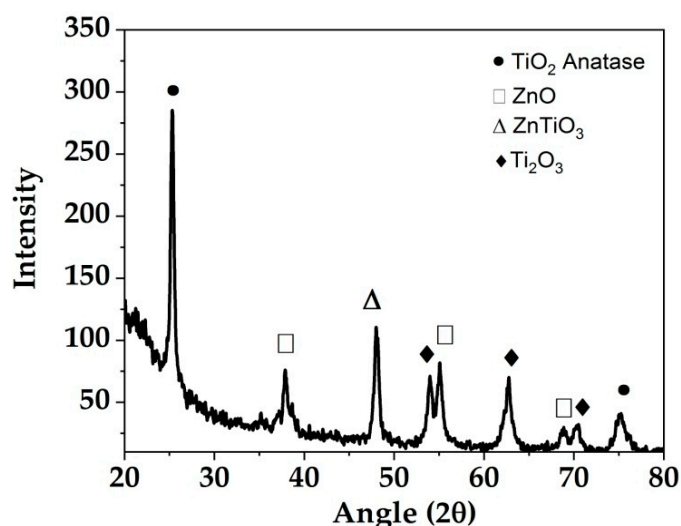


Figure 8. X-ray diffraction (XRD) pattern of TiO₂/ZnO nanofibers.

3.2. Photocatalytic Performance Evaluation

The photocatalytic reaction of TiO₂/ZnO is schematically shown in Figure 9. The electrons in the valence band can move to the conduction band and generate holes in the valence band by ultraviolet (UV) rays in sunlight. In heterojunction of ZnO with an energy band gap of 3.2 eV and TiO₂ with an energy band gap of 3.4 eV, the electrons in the conduction band of ZnO move to the conduction band of TiO₂; then the holes move from the valence band of TiO₂ to the valence band of ZnO. Electrons transferred to the TiO₂ conduction band react with O₂ to form a superoxide anion (O₂⁻). The holes transferred to the ZnO valence band react to form a strong hydroxyl radical (OH[•]). Such reactions continuously occur under UV irradiation, and high active radicals such as O₂⁻ and OH[•] can promote the photodegradation of organic pollutants [46–49]. Photodegradation characteristics using methylene blue were investigated for photocatalytic performance evaluation of TiO₂/ZnO nanofibers. TiO₂ nanofibers were used as a reference material to compare with TiO₂/ZnO nanofibers. All nanofibers were fabricated by the electrospinning process.

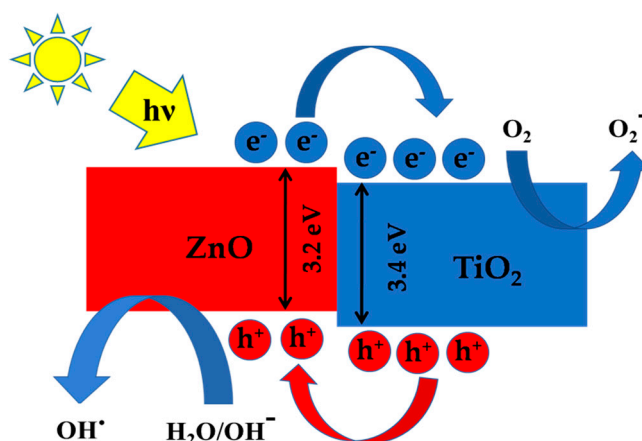


Figure 9. Illustration of photocatalytic mechanism in TiO_2/ZnO heterojunction [46].

Figure 10 shows the FE-SEM images of TiO_2 nanofibers and TiO_2/ZnO -1 and TiO_2/ZnO -2 nanofibers used in methylene blue photolysis experiments for photocatalytic performance evaluation. The microstructure in all nanofibers shows a typical one-dimensional nanofiber structure and their shapes are similar to each other. The diameters of TiO_2 , TiO_2/ZnO -1, and TiO_2/ZnO -2 nanofibers are 400 nm, 600 nm, and 400 nm, respectively. The diameters of TiO_2 nanofibers and TiO_2/ZnO -1 and TiO_2/ZnO -2 nanofibers are summarized in Table 3.

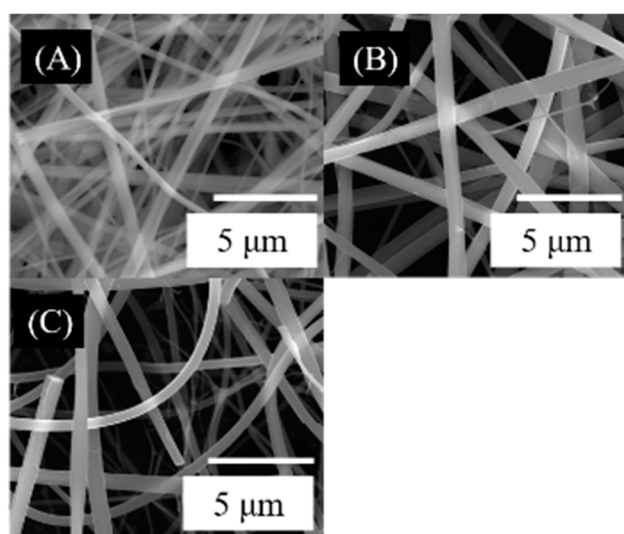


Figure 10. FE-SEM images of electrospinning process conditions of nanofibers used in the decomposition of methylene blue for photocatalytic performance evaluation: (A) TiO_2 nanofibers, (B) TiO_2/ZnO -1 nanofibers, (C) TiO_2/ZnO -2 nanofibers.

Table 3. The nanofibers used in the methylene blue decomposition experiments for photocatalytic performance evaluation.

Nanofibers	Diameter (nm)
TiO_2	400 ± 32
TiO_2/ZnO -1	600 ± 27
TiO_2/ZnO -2	400 ± 13

Figure 11 shows the absorption spectra to evaluate the photocatalytic performance of TiO_2/ZnO nanofibers observed by UV-Vis analysis. Figure 11a–d are the spectra of methylene blue without nanofibers, with TiO_2 nanofibers, with TiO_2/ZnO -1 nanofibers, and with TiO_2/ZnO -2 nanofibers,

respectively. A total of 0.5 g of nanofiber was added in a 200 mL methylene blue solution (Figure 11b–d). All spectra have peaks at wavelength of 291 nm, 611 nm, and 656 nm. The intensity of the peaks gradually decreased with time because some factors such as UV, TiO₂ nanofibers, and TiO₂/ZnO nanofibers, cause methylene blue to decompose. Since methylene blue shows a low absorbance when photolyzed by photocatalytic reaction, it is possible to know whether the photocatalytic reaction has occurred or not [50,51].

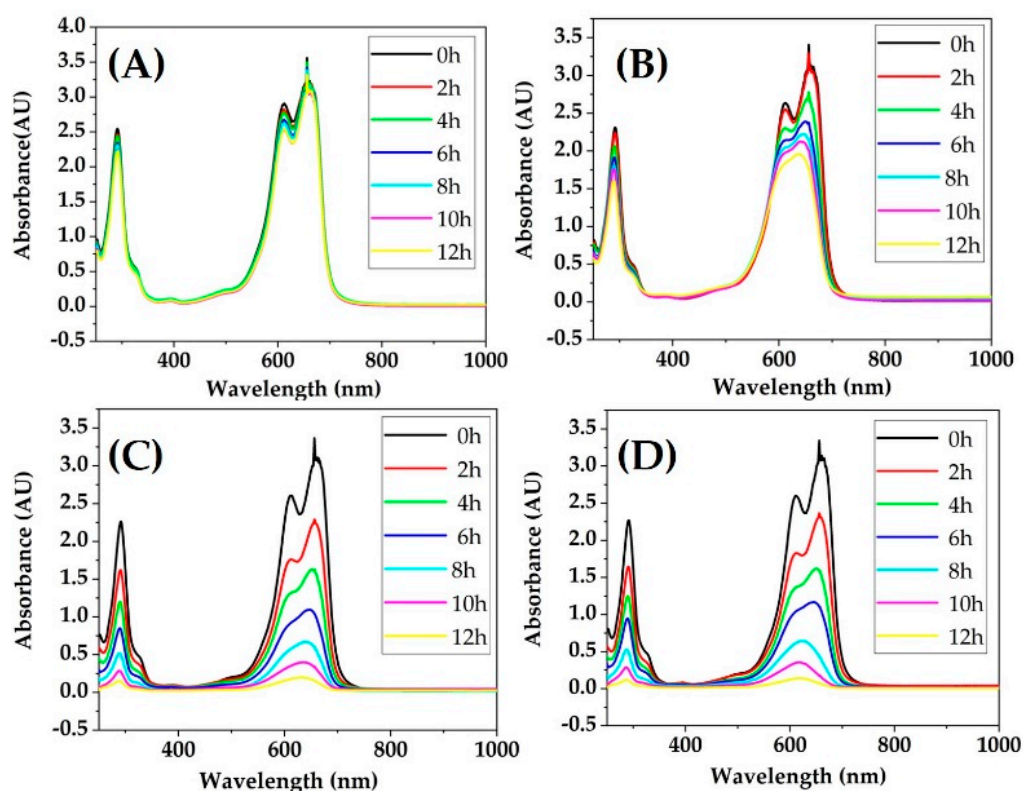


Figure 11. Ultraviolet–visible spectroscopy (UV–Vis) spectral change of photocatalytic decomposition of methylene blue over time using diameter-controlled nanofibers: (A) UV without nanofibers, (B) UV with 0.5 g TiO₂ nanofiber added, (C) UV with 0.5 g TiO₂/ZnO-1 nanofiber added, (D) UV with 0.5 g TiO₂/ZnO-2 nanofiber added.

To make sure methylene blue decomposed by photocatalytic reaction, the concentration of methylene blue on time was measured and normalized. The curves of normalized value (C/C_0) were plotted as shown in Figure 12. In methylene blue solution without TiO₂ nanofibers, the concentration very slowly decreased with time and only UV irradiation decomposed the methylene blue. After UV irradiation of 12 h, the normalized value of 0.874 was shown and the photodegradation rate was 12.6%. In methylene blue solution with TiO₂ nanofibers, the normalized value decreased to 0.581 and the photodegradation rate was 41.9%. In methylene blue solution with TiO₂/ZnO nanofibers, the normalized value dramatically decreased. This reveals that UV irradiation and photocatalytic reaction of TiO₂/ZnO nanofibers affect the decomposition of methylene blue. After UV irradiation of 12 h, the normalized values in methylene blue with TiO₂/ZnO-1 nanofibers and TiO₂-ZnO-2 nanofibers were 0.054 and 0.037 and a photodegradation rate of 94.6% and 96.3% were observed, respectively. The photodegradation rate in methylene blue with TiO₂/ZnO nanofibers was higher than with TiO₂ nanofibers. This shows that TiO₂/ZnO nanofibers decompose methylene blue more efficiently than TiO₂ nanofibers, and the photodegradability of TiO₂/ZnO nanofibers is better than that of TiO₂ nanofibers. The best photocatalytic decomposition performance for methylene blue was observed in methylene blue with TiO₂/ZnO-2 nanofibers. It was found that TiO₂/ZnO-2 nanofibers with a small diameter have better photolytic properties than TiO₂/ZnO-1 nanofibers [46–51].

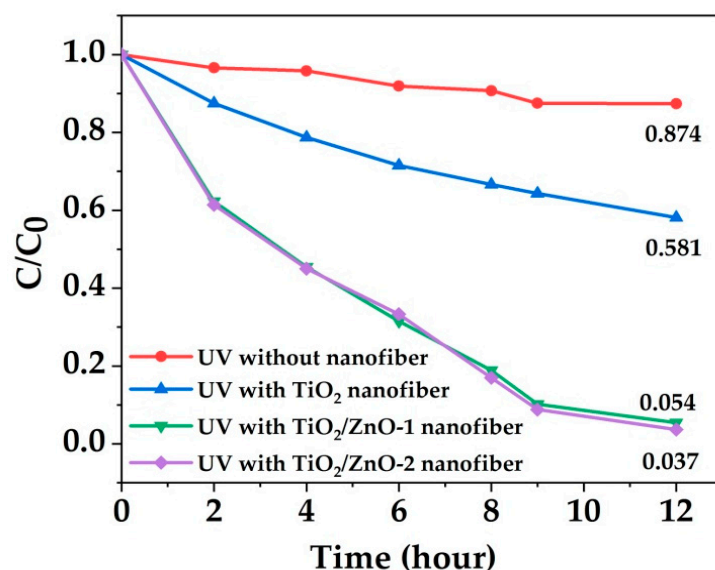


Figure 12. Photodegradation efficiency of TiO₂/ZnO nanofibers under UV irradiation for the decomposition of methylene blue.

4. Conclusions

One-dimensional TiO₂/ZnO nanofibers were fabricated by the electrospinning process with various process conditions. The voltage, inflow rate, and amount of acetic acid in precursor were controlled to obtain the optimized microstructure of TiO₂/ZnO nanofibers. The average diameter of TiO₂/ZnO nanofibers decreased with an increase in the applied voltage and amount of acetic acid and increased with inflow rate. Electrospun TiO₂/ZnO nanofibers have the crystalline structures of TiO₂ anatase, ZnO, Ti₂O₃, and ZnTiO₃. The best photocatalytic decomposition performance of methylene blue was observed in TiO₂/ZnO-2 nanofibers having a diameter of 400 nm. To increase the specific surface area in a way that improves the photocatalytic properties of these TiO₂/ZnO nanofibers, variables of the electrospinning process should be controlled to make the diameter small. Electrospun TiO₂/ZnO nanofibers with a small diameter will be excellent in photocatalytic properties and bio-friendly properties generated on a large specific surface area and will be utilized in various fields as well as in air pollution removal filters.

Author Contributions: Conceptualization, D.-C.P. and W.-Y.C.; methodology, C.-G.L.; validation, C.-G.L., K.-H.N., and W.-T.K.; formal analysis, C.-G.L.; investigation, C.-G.L.; resources, W.-H.Y. and W.-Y.C.; data curation, C.-G.L.; writing—original draft preparation, C.-G.L.; writing—review and editing, W.-Y.C.; visualization, K.-H.N. and W.-T.K.; supervision, W.-Y.C.; project administration, W.-H.Y. and W.-Y.C.; funding acquisition, D.-C.P. and W.-Y.C.

Funding: This work was supported by Gangneung-Wonju National University, Korea Institute of Energy Technology Evaluation and Planning (KETEP) and the Ministry of Trade, Industry and Energy (MOTIE) (Grant No. 20181110200070), Korea Agency for Infrastructure Technology Advancement under Construction Technology R&D project (Grant No. 18SCIP-B146646-01), and National Research Foundation of Korea (Grant No. 2019R111A3A01057765).

Acknowledgments: The authors thank the researchers (Tae-Hyeob Song and Jisun Park) of the Korea Institute of Civil Engineering and Building Technology, for their time and contributions to the study.

Conflicts of Interest: The authors declare no conflicts of interest.

References

- Griffiths, W.; Bennett, A.; Speight, S.; Parks, S. Determining the performance of a commercial air purification system for reducing airborne contamination using model micro-organisms: A new test methodology. *J. Hosp. Infect.* **2005**, *61*, 242–247. [[CrossRef](#)] [[PubMed](#)]
- Khalil, L.; Mourad, W.; Rophael, M. Photocatalytic reduction of environmental pollutant cr (vi) over some semiconductors under uv/visible light illumination. *Appl. Catal. B Environ.* **1998**, *17*, 267–273. [[CrossRef](#)]

3. Phillips, M.; Gleeson, K.; Hughes, J.M.B.; Greenberg, J.; Cataneo, R.N.; Baker, L.; McVay, W.P. Volatile organic compounds in breath as markers of lung cancer: A cross-sectional study. *Lancet* **1999**, *353*, 1930–1933. [[CrossRef](#)]
4. Fukuzumi, S.; Ohkubo, K. Selective photocatalytic reactions with organic photocatalysts. *Chem. Sci.* **2013**, *4*, 561–574. [[CrossRef](#)]
5. Hashimoto, K.; Kawai, T.; Sakata, T. Photocatalytic reactions of hydrocarbons and fossil fuels with water. Hydrogen production and oxidation. *J. Phys. Chem.* **1984**, *88*, 4083–4088. [[CrossRef](#)]
6. Ohko, Y.; Hashimoto, K.; Fujishima, A. Kinetics of photocatalytic reactions under extremely low-intensity uv illumination on titanium dioxide thin films. *J. Phys. Chem. A* **1997**, *101*, 8057–8062. [[CrossRef](#)]
7. Tachikawa, T.; Fujitsuka, M.; Majima, T. Mechanistic insight into the TiO₂ photocatalytic reactions: Design of new photocatalysts. *J. Phys. Chem. C* **2007**, *111*, 5259–5275. [[CrossRef](#)]
8. Behnajady, M.; Modirshahla, N.; Hamzavi, R. Kinetic study on photocatalytic degradation of ci acid yellow 23 by zno photocatalyst. *J. Hazard. Mater.* **2006**, *133*, 226–232. [[CrossRef](#)]
9. Jassby, D.; Farner Budarz, J.; Wiesner, M. Impact of aggregate size and structure on the photocatalytic properties of TiO₂ and ZnO nanoparticles. *Environ. Sci. Technol.* **2012**, *46*, 6934–6941. [[CrossRef](#)]
10. Miyauchi, M.; Nakajima, A.; Watanabe, T.; Hashimoto, K. Photocatalysis and photoinduced hydrophilicity of various metal oxide thin films. *Chem. Mater.* **2002**, *14*, 2812–2816. [[CrossRef](#)]
11. Ohno, T.; Sarukawa, K.; Tokieda, K.; Matsumura, M. Morphology of a TiO₂ photocatalyst (degussa, p-25) consisting of anatase and rutile crystalline phases. *J. Catal.* **2001**, *203*, 82–86. [[CrossRef](#)]
12. Qu, Y.; Duan, X. Progress, challenge and perspective of heterogeneous photocatalysts. *Chem. Soc. Rev.* **2013**, *42*, 2568–2580. [[CrossRef](#)] [[PubMed](#)]
13. Ramírez-Ortega, D.; Meléndez, A.M.; Acevedo-Peña, P.; González, I.; Arroyo, R. Semiconducting properties of zno/tio2 composites by electrochemical measurements and their relationship with photocatalytic activity. *Electrochim. Acta* **2014**, *140*, 541–549. [[CrossRef](#)]
14. Shan, G.; Yan, S.; Tyagi, R.; Surampalli, R.Y.; Zhang, T.C. Applications of nanomaterials in environmental science and engineering. *Pract. Period. Hazard. Toxic Radioact. Waste Manag.* **2009**, *13*, 110–119. [[CrossRef](#)]
15. William, L., IV; Kostedt, I.; Ismail, A.A.; Mazyck, D.W. Impact of heat treatment and composition of ZnO–TiO₂ nanoparticles for photocatalytic oxidation of an azo dye. *Ind. Eng. Chem. Res.* **2008**, *47*, 1483–1487.
16. Tang, H.; Yan, F.; Tai, Q.; Chan, H.L. The improvement of glucose bioelectrocatalytic properties of platinum electrodes modified with electrospun TiO₂ nanofibers. *Biosens. Bioelectron.* **2010**, *25*, 1646–1651. [[CrossRef](#)]
17. Gouma, P.-I. *Nanomaterials for Chemical Sensors and Biotechnology*; Pan Stanford Publishing: Singapore, 2010.
18. Lin, Z.-H.; Xie, Y.; Yang, Y.; Wang, S.; Zhu, G.; Wang, Z.L. Enhanced triboelectric nanogenerators and triboelectric nanosensor using chemically modified TiO₂ nanomaterials. *ACS Nano* **2013**, *7*, 4554–4560. [[CrossRef](#)]
19. Qiu, J.; Zhang, S.; Zhao, H. Recent applications of TiO₂ nanomaterials in chemical sensing in aqueous media. *Sens. Actuators B Chem.* **2011**, *160*, 875–890. [[CrossRef](#)]
20. Bignozzi, C.A.; Dissette, V. Material, Item and Products Comprising a Composition Having Anti-Microbial Properties. U.S. Patent No. 8,389,022, 5 March 2013.
21. Bian, S.-W.; Mudunkotuwa, I.A.; Rupasinghe, T.; Grassian, V.H. Aggregation and dissolution of 4 nm zno nanoparticles in aqueous environments: Influence of ph, ionic strength, size, and adsorption of humic acid. *Langmuir* **2011**, *27*, 6059–6068. [[CrossRef](#)]
22. Wu, C.-M.; Baltrusaitis, J.; Gillan, E.G.; Grassian, V.H. Sulfur dioxide adsorption on zno nanoparticles and nanorods. *J. Phys. Chem. C* **2011**, *115*, 10164–10172. [[CrossRef](#)]
23. Weintraub, B.; Zhou, Z.; Li, Y.; Deng, Y. Solution synthesis of one-dimensional zno nanomaterials and their applications. *Nanoscale* **2010**, *2*, 1573–1587. [[CrossRef](#)] [[PubMed](#)]
24. Chopra, N.; Gavalas, V.G.; Bachas, L.G.; Hinds, B.J.; Bachas, L.G. Functional one-dimensional nanomaterials: Applications in nanoscale biosensors. *Anal. Lett.* **2007**, *40*, 2067–2096. [[CrossRef](#)]
25. Gibson, P.; Schreuder-Gibson, H.; Rivin, D. Transport properties of porous membranes based on electrospun nanofibers. *Colloids Surf. A Physicochem. Eng. Asp.* **2001**, *187*, 469–481. [[CrossRef](#)]
26. Long, Y.-Z.; Li, M.-M.; Gu, C.; Wan, M.; Duvail, J.-L.; Liu, Z.; Fan, Z. Recent advances in synthesis, physical properties and applications of conducting polymer nanotubes and nanofibers. *Prog. Polym. Sci.* **2011**, *36*, 1415–1442. [[CrossRef](#)]

27. Hwang, T.-H.; Kim, W.-T.; Choi, W.-Y. Photoconversion of dye-sensitized solar cells with a 3d-structured photoelectrode consisting of both TiO₂ nanofibers and nanoparticles. *J. Electron. Mater.* **2016**, *45*, 3195–3199. [[CrossRef](#)]
28. Kim, B.-Y.; Yoon, J.-W.; Lee, C.; Park, J.-S.; Lee, J.-H. Trimethylamine sensing characteristics of molybdenum doped ZnO hollow nanofibers prepared by electrospinning. *J. Sens. Sci. Technol.* **2015**, *24*, 419–422. [[CrossRef](#)]
29. Kim, W.-T.; Choi, W.-Y. Fabrication of TiO₂ photonic crystal by anodic oxidation and their optical sensing properties. *Sens. Actuators A Phys.* **2017**, *260*, 178–184. [[CrossRef](#)]
30. Choi, W.-Y.; Chung, J.; Cho, C.-H.; Kim, J.-O. Fabrication and photocatalytic activity of a novel nanostructured TiO₂ metal membrane. *Desalination* **2011**, *279*, 359–366. [[CrossRef](#)]
31. Hu, J.; Odom, T.W.; Lieber, C.M. Chemistry and physics in one dimension: Synthesis and properties of nanowires and nanotubes. *Acc. Chem. Res.* **1999**, *32*, 435–445. [[CrossRef](#)]
32. Lu, X.; Wang, C.; Wei, Y. One-dimensional composite nanomaterials: Synthesis by electrospinning and their applications. *Small* **2009**, *5*, 2349–2370. [[CrossRef](#)]
33. Ramaseshan, R.; Sundarajan, S.; Jose, R.; Ramakrishna, S. Nanostructured ceramics by electrospinning. *J. Appl. Phys.* **2007**, *102*, 7. [[CrossRef](#)]
34. Hwang, T.-H.; Kim, W.-T.; Choi, W.-Y. Mixed dimensionality with a TiO₂ nanostructure and carbon nanotubes for the photoelectrode in dye-sensitized solar cells. *J. Nanosci. Nanotechnol.* **2017**, *17*, 4812–4816. [[CrossRef](#)]
35. Kim, W.-T.; Hwang, T.-H.; Choi, W.-Y. Composite photoelectrode with TiO₂ nanofibers and nanoparticles in dye-sensitized solar cells. *Sci. Adv. Mater.* **2018**, *10*, 210–214. [[CrossRef](#)]
36. Nakata, K.; Fujishima, A. TiO₂ photocatalysis: Design and applications. *J. Photochem. Photobiol. C Photochem. Rev.* **2012**, *13*, 169–189. [[CrossRef](#)]
37. Zhang, M.; Shao, C.; Mu, J.; Zhang, Z.; Guo, Z.; Zhang, P.; Liu, Y. One-dimensional Bi₂MoO₆/TiO₂ hierarchical heterostructures with enhanced photocatalytic activity. *CrystEngComm* **2012**, *14*, 605–612. [[CrossRef](#)]
38. Li, H.; Zhang, W.; Li, B.; Pan, W. Diameter-dependent photocatalytic activity of electrospun TiO₂ nanofiber. *J. Am. Ceram. Soc.* **2010**, *93*, 2503–2506. [[CrossRef](#)]
39. Doshi, J.; Reneker, D.H. Electrospinning process and applications of electrospun fibers. *J. Electrostat.* **1995**, *35*, 151–160. [[CrossRef](#)]
40. Ramakrishna, S. *An Introduction To Electrospinning And Nanofibers*; World Scientific: Singapore, 2005.
41. Luo, C.; Stoyanov, S.D.; Stride, E.; Pelan, E.; Edirisinghe, M. Electrospinning versus fibre production methods: From specifics to technological convergence. *Chem. Soc. Rev.* **2012**, *41*, 4708–4735. [[CrossRef](#)]
42. Persano, L.; Camposeo, A.; Tekmen, C.; Pisignano, D. Industrial upscaling of electrospinning and applications of polymer nanofibers: A review. *Macromol. Mater. Eng.* **2013**, *298*, 504–520. [[CrossRef](#)]
43. Nayak, R.; Padhye, R.; Kyratzis, I.L.; Truong, Y.B.; Arnold, L. Recent advances in nanofibre fabrication techniques. *Text. Res. J.* **2012**, *82*, 129–147. [[CrossRef](#)]
44. Bognitzki, M.; Czado, W.; Frese, T.; Schaper, A.; Hellwig, M.; Steinhart, M.; Greiner, A.; Wendorff, J.H. Nanostructured fibers via electrospinning. *Adv. Mater.* **2001**, *13*, 70–72. [[CrossRef](#)]
45. Spivak, A.; Dzenis, Y.; Reneker, D. Model of steady state jet in the electrospinning process. *Mech. Res. Commun.* **2000**, *27*, 37–42. [[CrossRef](#)]
46. Liu, R.; Ye, H.; Xiong, X.; Liu, H. Fabrication of TiO₂/ZnO composite nanofibers by electrospinning and their photocatalytic property. *Mater. Chem. Phys.* **2010**, *121*, 432–439. [[CrossRef](#)]
47. Wang, S.; Yun, J.-H.; Luo, B.; Butburee, T.; Peerakiatkhajohn, P.; Thaweesak, S.; Xiao, M.; Wang, L. Recent progress on visible light responsive heterojunctions for photocatalytic applications. *J. Mater. Sci. Technol.* **2017**, *33*, 1–22. [[CrossRef](#)]
48. Ke, J.; Younis, M.A.; Kong, Y.; Zhou, H.; Liu, J.; Lei, L.; Hou, Y. Nanostructured ternary metal tungstate-based photocatalysts for environmental purification and solar water splitting: A review. *Nano-Micro Lett.* **2018**, *10*, 69. [[CrossRef](#)]
49. Wang, H.; Zhang, L.; Chen, Z.; Hu, J.; Li, S.; Wang, Z.; Liu, J.; Wang, X. Semiconductor heterojunction photocatalysts: Design, construction, and photocatalytic performances. *Chem. Soc. Rev.* **2014**, *43*, 5234–5244. [[CrossRef](#)]

50. Ullah, R.; Dutta, J. Photocatalytic degradation of organic dyes with manganese-doped ZnO nanoparticles. *J. Hazard. Mater.* **2008**, *156*, 194–200. [[CrossRef](#)]
51. Yogi, C.; Kojima, K.; Wada, N.; Tokumoto, H.; Takai, T.; Mizoguchi, T.; Tamiaki, H. Photocatalytic degradation of methylene blue by TiO₂ film and Au particles-TiO₂ composite film. *Thin Solid Film.* **2008**, *516*, 5881–5884. [[CrossRef](#)]



© 2019 by the authors. Licensee MDPI, Basel, Switzerland. This article is an open access article distributed under the terms and conditions of the Creative Commons Attribution (CC BY) license (<http://creativecommons.org/licenses/by/4.0/>).